

Hierarchical Divergence Conforming Bases for Edge Singularities in Quadrilateral Cells

*Original*

Hierarchical Divergence Conforming Bases for Edge Singularities in Quadrilateral Cells / Graglia, R. D.; Peterson, A. F.; Petrini, P.. - In: IEEE TRANSACTIONS ON ANTENNAS AND PROPAGATION. - ISSN 0018-926X. - ELETTRONICO. - 66:11(2018), pp. 6191-6201. [10.1109/TAP.2018.2854298]

*Availability:*

This version is available at: 11583/2716084 since: 2018-11-21T10:20:12Z

*Publisher:*

IEEE

*Published*

DOI:10.1109/TAP.2018.2854298

*Terms of use:*

This article is made available under terms and conditions as specified in the corresponding bibliographic description in the repository

*Publisher copyright*

(Article begins on next page)

# Hierarchical Divergence Conforming Bases for Edge Singularities in Quadrilateral Cells

Roberto D. Graglia, *Fellow, IEEE*, Andrew F. Peterson, *Fellow, IEEE*, and Paolo Petrini

**Abstract**—Singular divergence-conforming bases have been proposed for the solution of integral equations although they have seen only occasional use in practical applications. The existing singular bases are not hierarchical, which prevents their use in adaptive  $p$ -refinement applications. In this article, a new family of singular hierarchical basis functions is proposed for quadrilateral cells. These functions model the singularities associated with current and charge density at edges and are more convenient for modeling such singularities than triangular bases of the same kind. The basis functions are of the additive kind, and combine a hierarchical polynomial representation on quadrilaterals with linearly independent singular terms that incorporate general exponents that may be adjusted for the specific wedge angle of interest. Moreover, the added singular basis functions are computed on the fly. On the basis of various reported numerical results, the present work also illustrates the difficulties, the advantages, the accuracy, and the cost of using such bases in Method of Moments solutions of integral equations.

**Index Terms** – Basis Functions, Hierarchical Basis Functions, Method of Moments, Singular basis functions, Wedges.

## I. INTRODUCTION

The electromagnetic surface charge and current densities, and certain field components, can be singular and sometimes infinite in the vicinity of conducting or penetrable edges and corners [1]. Although this behavior is localized at the edge or corner, it stresses the accuracy and raises the computational cost of numerical solvers. One possibility to improve the quality of the results is to use a denser mesh or to adaptively refine the cell sizes ( $h$ -refinement) in the neighborhood of the singular region [2]. Adaptive  $h$ -refinement is commonly used by modern Finite Element Method (FEM) solvers to achieve polynomial convergence in the solution of differential problems. For integral equation problems, Method of Moments (MoM) solvers often use denser meshes in the neighborhood of edges and corners but rarely use adaptive  $h$ -refinement, perhaps because of increased costs associated with the dense nature of the MoM system matrices. An alternative that is expected to produce exponential convergence in numerical applications is known as  $p$ -refinement, which requires the introduction of singular basis functions to treat fields near

edges. (A combination of  $h$  and  $p$  refinement may prove optimal [3], [4].)

Most existing singular basis functions can be classified as either *substitutive* or *additive* functions [5]. For low-order numerical techniques, substitutive bases (specially constructed singular functions that replace the original basis functions on a 1:1 ratio) can be effective. Substitutive vector bases for edge singularities on triangular cells were proposed by Brown and Wilton [6], Graglia and Lombardi [7] and Ozturk et al. [8], while bases for quadrilateral cells were proposed by Andersson [9] and Graglia and Lombardi [7]. Conversely, an additive representation is obtained by augmenting the regular polynomial vector bases with additional independent degrees of freedom to model the singular field behavior [10]. For high-order treatment, basis functions of the additive kind provide improved accuracy and additional flexibility since one can model appropriate field behavior even if the expected singularity is not excited by the source. Most of all, whenever the polynomial basis subset is hierarchical (a polynomial basis is hierarchical if the functions used for order  $p-1$  are a subset of those used for order  $p$ ), additive bases allow  $p$ -refinement up to the polynomial order  $p$  for which the polynomial functions remain linearly independent from the singular ones. The reader is referred to [5], [11], and the references therein for more details.

The present paper proposes hierarchical vector basis functions for the numerical treatment of edge singularities in the context of two-dimensional quadrilateral-cell MoM analysis. The basis functions presented here improve upon those discussed in [10] where interpolatory polynomials were used to build high-order, non-hierarchical bases. The functions under consideration are divergence conforming and impose normal-vector continuity across cell boundaries. They are primarily designed for the solution of the Electric Field Integral Equation (EFIE) where it is necessary to represent both the unknown current density and its divergence.

Specific issues discussed here include the following:

- The Degrees of Freedom (DoF) associated with additive basis sets formed by the combination of regular and singular basis functions.
- The error reduction due to the use of singular basis functions.
- Deterioration of the matrix condition number due to the singular basis function subsets.

A companion paper [12] describes numerical integration techniques used to compute the MoM source integrals involving singular basis functions.

Manuscript received January 29, 2018; revised May 27, 2018.

R.D. Graglia is with the Dipartimento di Elettronica e Telecomunicazioni, Politecnico di Torino, Corso Duca degli Abruzzi 24, 10129 Torino, Italy (email: roberto.graglia@polito.it).

A.F. Peterson is with the School of Electrical and Computer Engineering, Georgia Institute of Technology, Atlanta, GA 30332 USA (email: peterson@ece.gatech.edu).

P. Petrini is with the Dipartimento di Elettronica e Telecomunicazioni, Politecnico di Torino, Corso Duca degli Abruzzi 24, 10129 Torino, Italy (email: paolo.petrini@polito.it).

TABLE I  
ZERO-TH-ORDER, DIVERGENCE-CONFORMING BASES FOR THE QUADRILATERAL CELL

Basis Functions	Surface Divergences	Dependency Relations
Regular Functions [11], [13] $\Lambda_\beta(\mathbf{r}) = \frac{\xi_{\beta+2} \ell_{\beta-1}}{\mathcal{J}} \quad \text{for } \beta = 1, 2, 3, \text{ and } 4$	$\frac{1}{\mathcal{J}}$	$\xi_1 \Lambda_1(\mathbf{r}) + \xi_3 \Lambda_3(\mathbf{r}) = 0$ $\xi_2 \Lambda_2(\mathbf{r}) + \xi_4 \Lambda_4(\mathbf{r}) = 0$
Singular Functions [10], [11] ${}^e\Lambda_{i\pm 1}(\mathbf{r}) = \left( \nu \xi_i^{\nu-1} - 1 \right) \Lambda_{i\pm 1}(\mathbf{r})$ ${}^e\mathbf{V}_{i+2}(\mathbf{r}) = \left( \xi_i^{\nu-1} - 1 \right) \Lambda_{i+2}(\mathbf{r}) \quad \text{for } i = 1, 2, 3, \text{ or } 4$	$\frac{\nu \xi_i^{\nu-1} - 1}{\mathcal{J}}$	$\xi_{i+1} {}^e\Lambda_{i+1}(\mathbf{r}) + \xi_{i-1} {}^e\Lambda_{i-1}(\mathbf{r}) = 0$
The subscripts are counted modulo 4, for $\beta$ and $i = 1, 2, 3$ or $4$ . $\mathcal{J}$ is the Jacobian of the transformation from parent to child space. The functions ${}^e\Lambda_{i\pm 1}$ are singular on the $i$ -th edge (where $\xi_i = 0$ ), and vanish for $\nu = 1$ . $\Lambda_\beta$ and ${}^e\Lambda_{i\pm 1}$ are edge-based and associated only with the edge quoted in their subscript, since the normal component of these functions along the other element edges (not quoted in the subscript) is always equal to zero. Conversely, ${}^e\mathbf{V}_{i+2}$ is a <i>bubble</i> (element-based) function with a vanishing normal component along each of the element edges, but with singular surface divergence at $\xi_i = 0$ . To reflect the edgeless property, the symbol ${}^e\mathbf{V}_{i+2}$ has been obtained by overturning $\Lambda$ , while the subscript indicates that ${}^e\mathbf{V}_{i+2}$ is given in terms of the regular function $\Lambda_{i+2}$ .		

Section II provides sufficient information to understand the numerical results presented in sections IV and V without requiring the readers to study the theory and other mathematical details associated with the new basis functions, which are developed in Section III. Readers interested in the theory may find it helpful to review [10], [11], and [13] for a detailed introduction to the notation and other important background information.

Preliminary results of this research work were presented in [14], [15].

## II. BASIS FUNCTION SETS AND THEIR ORDER

The basis functions and the cells are described in terms of four local or parent variables  $\xi_\beta$  (for  $\beta = 1$  to  $4$ , and indexes counted modulo 4), two of which are independent with

$$\xi_\beta + \xi_{\beta+2} = 1 \quad (1)$$

Variable  $\xi_\beta$  vanishes on the  $\beta$ -th edge of the cell along the coordinate-line  $\xi_\beta = 0$ . If a cell has a singular edge this is denoted by the subscript  $i$ , so that the variable  $\xi_i$  vanishes on the singular edge; in this case the two parent variables  $\xi_{i\pm 1}$  are *longitudinal* in the sense that they vary from 0 to +1 in directions tangential to the singular edge.

Singular vector basis functions are constructed from scalar functions of the independent ( $\xi_i$ ) and longitudinal ( $\xi_{i\pm 1}$ ) variables using the fundamental singular factors

$$f_A(\nu) = \nu \xi_i^{\nu-1} - 1 \quad (2)$$

$$f_B(\nu) = \xi_i^{\nu-1} - 1 \quad (3)$$

where  $\nu$  is any entry of the finite list

$$\boldsymbol{\nu} = \{\nu_1, \nu_2, \dots, \nu_j, \dots, \nu_s\} \quad (4)$$

formed by the first  $s$  smallest *non-integer* singularity coefficients that appear in the infinite set of exponents that form the complete expansion of the electromagnetic field near the singular edge [1], [5]. The functions (2, 3) obtained by using the  $\nu$  values in (4) are not orthogonal. To obtain orthogonal singular factors of  $\xi_i$  it is sufficient to add to  $f_A$  and  $f_B$  some

appropriate polynomials of  $\xi_i$  whose maximum order is  $(s-1)$ . The resulting orthogonal factors are then multiplied by the zero-th order regular vector basis functions and by orthogonal polynomials of maximum order  $m$  of the longitudinal parent variable, to obtain the vector singular basis functions (for full details, see Section III). The order of the singular set formed in this manner, the so-called Meixner subset [11], is denoted by the integers  $[s, m]$ .

Thus, we describe the order of the additive quadrilateral basis by three integers  $[p, s, m]$ , where  $p$  is the order of the vector polynomial basis (the *background* polynomial order of the expansion),  $s$  is the number of fractional exponents from (4) included in the representation, and  $m$  is the order of the singular basis subset in the longitudinal direction. We expect that  $m = p$  will provide the most consistent representation.

The polynomial and the Meixner subsets are built using orthogonal polynomials to ensure linear independence of the basis functions and attempt to maintain a well-conditioned MoM matrix.

We observe that edge singularities may be easier to properly model using quadrilateral elements than triangular ones because the latter require the introduction of “element fillers” (that is, vertex singularity triangles) with only one vertex attached to the singular edge [10, Section III-D]. As discussed in [10, Section III-D], bases on such cells require additional information to align them with the edge and may reduce accuracy. On the contrary, it may be easier to model *corner singularities* in MoM analysis by adjacent singular triangular elements instead of quadrilateral cells; the quadrilateral bases presented here are not designed to model corner singularities that depend on the distance from the corner’s tip instead of the distance from the two corner’s edges [5], [18] (Triangular elements have also been used to model sharp edge junctions in [16].)

## III. SINGULAR HIERARCHICAL BASES

Table I summarizes the lowest-order divergence-conforming basis functions for the quadrilateral cell discussed in [10], [11], [13]. Table II reports the hierarchical generalization of those

TABLE II  
HIERARCHICAL DIVERGENCE-CONFORMING BASES FOR THE QUADRILATERAL CELL

	Basis Functions	Surface Divergences	Orthogonality Relations
Polynomial Set	Edge Functions $\Lambda_{0k}^\beta(\mathbf{r}) = H_{0k}(\xi) \Lambda_\beta(\mathbf{r})$ $k = 0, 1, \dots, p; \beta = 1, \dots, 4.$	$\frac{H_{0k}(\xi)}{\mathcal{J}}$	$\iint_{\text{parent-cell}} \Lambda_{0k}^\beta \cdot \Lambda_{0h}^\beta d\xi = \frac{1}{3} \delta_{kh}$
	Bubble Functions $\Lambda_{jk}^\beta(\mathbf{r}) = H_{jk}(\xi) \Lambda_\beta(\mathbf{r})$ $k = 0, 1, \dots, p; j = 1, 2, \dots, p; \beta = 1, 2.$	$\frac{H_{0k}(\xi)}{\mathcal{J}} g_{j-1}(\xi_\beta - \xi_{\beta+2})$	$\iint_{\text{parent-cell}} \Lambda_{jk}^\beta \cdot \Lambda_{\ell h}^\beta d\xi = \frac{1}{3} \delta_{kh} \delta_{j\ell}$
	$\Lambda_\beta(\mathbf{r})$ indicates the zeroth-order regular functions of Table I. $\delta_{kh}, \delta_{j\ell}$ denote the Kronecker delta. The vector functions are defined in terms of the scalar polynomials $H_{0k}(\xi) = E_k(\xi_{\beta+1} - \xi_{\beta-1})$ $H_{jk}(\xi) = \xi_\beta f_{j-1}(\xi_\beta - \xi_{\beta+2}) H_{0k}(\xi)$		
	The $E_k, f_n$ , and $g_n$ polynomials of Table III yield the reported orthogonality relations valid for integrals on the square part-cell. The $p$ -th order complete edge-based and bubble subsets have $4(p+1)$ and $2p(p+1)$ DoFs, respectively, for a total of $2(p+1)(p+2)$ DoFs.		
Singular Set	Basis Functions and Their Surface Divergence		Orthogonality Relations
	Edge Functions ${}^e\Lambda_{j0}^{i\pm 1}(\mathbf{r}) = N_{j-1}^a \sqrt{3} \left[ (\nu_j \xi_i^{\nu_j-1} - 1) + A_{j-1}(\xi_i) \right] \Lambda_{i\pm 1}(\mathbf{r})$ $\nabla \cdot {}^e\Lambda_{j0}^{i\pm 1}(\mathbf{r}) = \frac{N_{j-1}^a}{\mathcal{J}} \sqrt{3} \left[ (\nu_j \xi_i^{\nu_j-1} - 1) + A_{j-1}(\xi_i) \right]$		$\iint_{\text{parent-cell}} {}^e\Lambda_{j0}^{i\pm 1} \cdot \Lambda_{0h}^{i\pm 1} d\xi = 0 \quad \forall j$ $\iint_{\text{parent-cell}} {}^e\Lambda_{j0}^{i\pm 1} \cdot \Lambda_{\ell h}^{i\pm 1} d\xi = 0 \quad \forall \ell \geq 1$
	Bubble Functions ${}^e\Lambda_{jk}^{i+1}(\mathbf{r}) = N_{j-1}^a \left[ (\nu_j \xi_i^{\nu_j-1} - 1) + A_{j-1}(\xi_i) \right] [\xi_{i+1} f_{k-1}(z)] \Lambda_{i+1}(\mathbf{r})$ ${}^e\mathbf{V}_{j0}^{i+2}(\mathbf{r}) = N_{j-1}^b \left[ (\nu_j \xi_i^{\nu_j-1} - 1) + B_{j-1}(\xi_i) \right] \Lambda_{i+2}(\mathbf{r})$ ${}^e\mathbf{V}_{jk}^{i+2}(\mathbf{r}) = N_{j-1}^b \left[ (\nu_j \xi_i^{\nu_j-1} - 1) + B_{j-1}(\xi_i) \right] E_k(z) \Lambda_{i+2}(\mathbf{r})$ $\nabla \cdot {}^e\Lambda_{jk}^{i+1}(\mathbf{r}) = \frac{N_{j-1}^a}{\mathcal{J}} \left[ (\nu_j \xi_i^{\nu_j-1} - 1) + A_{j-1}(\xi_i) \right] g_{k-1}(z)$ $\nabla \cdot {}^e\mathbf{V}_{j0}^{i+2}(\mathbf{r}) = \frac{N_{j-1}^b}{\mathcal{J}} \left[ (\nu_j \xi_i^{\nu_j-1} - 1) + \frac{d}{d\xi_i} [\xi_i B_{j-1}(\xi_i)] \right]$ $\nabla \cdot {}^e\mathbf{V}_{jk}^{i+2}(\mathbf{r}) = \frac{N_{j-1}^b}{\mathcal{J}} \left[ (\nu_j \xi_i^{\nu_j-1} - 1) + \frac{d}{d\xi_i} [\xi_i B_{j-1}(\xi_i)] \right] E_k(z)$		$\iint_{\text{parent-cell}} {}^e\Lambda_{jk}^{i+1} \cdot \Lambda_{0h}^{i\pm 1} d\xi = 0 \quad \forall j$ $\iint_{\text{parent-cell}} {}^e\Lambda_{jk}^{i+1} \cdot \Lambda_{\ell h}^{i\pm 1} d\xi = 0 \quad \text{for } k \neq h$ $\iint_{\text{parent-cell}} {}^e\Lambda_{jk}^{i+1} \cdot {}^e\Lambda_{\ell h}^{i+1} d\xi = 0 \quad \text{for } j \neq \ell \text{ or } k \neq h$ $\iint_{\text{parent-cell}} {}^e\mathbf{V}_{jk}^{i+2} \cdot {}^e\mathbf{V}_{\ell h}^{i+2} d\xi = 0 \quad \text{for } j \neq \ell \text{ or } k \neq h$
	for $j = 1, 2, \dots, s; k = 1, 2, \dots, m$ with $s-1, m \leq p$		
	The functions model the behavior of the $s$ different, non-integer singularity coefficients $\{\nu_1, \nu_2, \dots, \nu_s\}$ . The indexes $i \pm 1, i + 2$ are counted modulo 4, for $i = 1, 2, 3$ or 4. The $E_n, f_n$ , and $g_n$ polynomials of Table III yield the reported orthogonality relations valid for integrals on the square parent-cell, with $z = \xi_{i+1} - \xi_{i-1}, \quad \xi_{i\pm 1} = \frac{1 \pm z}{2}$		

basis functions to high orders while providing  $s$  different, non-integer singularity coefficients  $\{\nu_1, \nu_2, \dots, \nu_j, \dots, \nu_s\}$ . To help maintain linear independence, both the polynomial and singular basis functions incorporate orthogonal polynomials that are defined in Table III.

The function  $\Lambda_\beta$  is independent of variables  $\xi_{\beta+1}$  and  $\xi_{\beta-1}$  on the parent cell, is linear in  $\xi_\beta = (1 - \xi_{\beta+2})$ , and vanishes at  $\xi_\beta = 1$ . The hierarchical polynomial high-order subset  $\Lambda_{0k}^\beta$  reported at top of Table II is constructed by multiplying the  $\Lambda_\beta$  functions with a scalar set of orthogonal (shifted-Legendre) polynomials of the  $\xi_{\beta+1} = (1 - \xi_{\beta-1})$  variable. In this manner, the function  $\Lambda_{0k}^\beta$  remains edge-based and has the same order in  $\xi_\beta$  as  $\Lambda_\beta$ , with  $\Lambda_{00}^\beta = \Lambda_\beta$ .

To model high-order (polynomial) variations along  $\xi_\beta$ , one

must introduce the hierarchical polynomial subset given in the second row of Table II, obtained by further multiplying each  $\Lambda_{0k}^\beta$  function by a set of modified orthogonal Jacobi polynomials [11]. Thus, a  $p$ -th order complete vector polynomial set is obtained from the Cartesian product of two  $p$ -th order scalar polynomial sets (one for each of the two independent variables) by eliminating from the bubble-function set, at the end of the construction process, any redundancy due to the dependency relations of Table I; that is, for example, by eliminating all the bubble functions  $\Lambda_{jk}^\beta$  obtained with  $\beta = 3, 4$ . The number of Degrees of Freedom (DoF) associated with the polynomial  $p$ -th order set is therefore equal to  $2(p+1)(p+2)$  [11].

The singular basis function sets at the bottom of Table II

TABLE III  
GENERATING ORTHOGONAL POLYNOMIALS

Recurrence Relations with Respect to the Degree $n$ $a_{1n}P_{n+1}^{(\alpha,\beta)}(z) = a_{2n}zP_n^{(\alpha,\beta)}(z) - a_{3n}P_{n-1}^{(\alpha,\beta)}(z)$	Generating Polynomials, Scale Factors $N_n$ and Integral Normalizations [17]
<p>Legendre <math>P_n(z)</math></p> <p><math>P_0(z) = 1</math> <span style="margin-left: 100px;"><math>a_{1n} = n + 1</math></span></p> <p><math>P_1(z) = z</math> <span style="margin-left: 100px;"><math>a_{2n} = 2n + 1</math></span></p> <p><math>P_2(z) = \frac{1}{2}(3z^2 - 1)</math> <span style="margin-left: 100px;"><math>a_{3n} = n</math></span></p>	<p style="text-align: center;"><math>E_n(z) = \sqrt{2n+1} P_n(z)</math></p> <hr/> <p style="text-align: center;"><math>\frac{1}{2} \int_{-1}^1 E_n^2(z) dz = \int_0^1 E_n^2(2x-1) dx = 1</math></p>
<p>Jacobi <math>P_n^{(2,2)}(z)</math></p> <p><math>P_0^{(2,2)}(z) = 1</math> <span style="margin-left: 100px;"><math>a_{1n} = (n+1)(n+5)</math></span></p> <p><math>P_1^{(2,2)}(z) = 3z</math> <span style="margin-left: 100px;"><math>a_{2n} = (n+3)(2n+5)</math></span></p> <p><math>P_2^{(2,2)}(z) = 7z^2 - 1</math> <span style="margin-left: 100px;"><math>a_{3n} = (n+2)(n+3)</math></span></p> <p>Jacobi <math>P_n^{(3,3)}(z)</math></p> <p><math>P_0^{(3,3)}(z) = 1</math> <span style="margin-left: 100px;"><math>a_{1n} = (n+1)(n+7)</math></span></p> <p><math>P_1^{(3,3)}(z) = 4z</math> <span style="margin-left: 100px;"><math>a_{2n} = (n+4)(2n+7)</math></span></p> <p><math>P_2^{(3,3)}(z) = \frac{5}{4}(9z^2 - 1)</math> <span style="margin-left: 100px;"><math>a_{3n} = (n+3)(n+4)</math></span></p>	<p style="text-align: center;"><math>N_n^f = \sqrt{\frac{(2n+5)(n+3)(n+4)}{3(n+1)(n+2)}}</math></p> <p style="text-align: center;"><math>f_n(z) = N_n^f P_n^{(2,2)}(z)</math></p> <p style="text-align: center;"><math>g_n(z) = N_n^f [zP_n^{(2,2)}(z) + h_n(z)]</math></p> <p style="text-align: center;"><math>h_n(z) = \frac{(z^2-1)}{2} \frac{dP_n^{(2,2)}(z)}{dz} = (n+5) \frac{(z^2-1)}{4} P_{n-1}^{(3,3)}(z)</math></p> <hr/> <p style="text-align: center;"><math>\frac{1}{2} \int_{-1}^1 \left[ \frac{1-z^2}{4} f_n(z) \right]^2 dz = \frac{1}{3}</math></p> <p style="text-align: center;"><math>\frac{1}{2} \int_{-1}^1 \frac{1-z^2}{4} h_n^2(z) dz = \frac{n(n+5)}{3 (N_n^f)^2}</math></p>
<p><math>P_n(z)</math> and <math>P_n^{(\alpha,\beta)}(z)</math> are the Legendre and the Jacobi polynomial of order <math>n</math>, respectively; with <math>P_n(z) = P_n^{(0,0)}(z)</math> and <math>P_n^{(\beta,\alpha)}(z) = (-1)^n P_n^{(\alpha,\beta)}(-z)</math>. The order of the polynomials is indicated by their subscripts with the only exception of the generating polynomials <math>g_n(z)</math> and <math>h_n(z)</math> whose order is equal to <math>(n+1)</math>. This convention is convenient because <math>g_n(z)</math> and <math>h_n(z)</math> are paired with <math>f_n(z)</math> whose order is <math>n</math>. (<math>g_n(z)</math> and <math>h_n(z)</math> are used to compute the divergence of the functions of Table II that contain the <math>(n+1)</math>-order factor <math>\xi f_n(z)</math>.)</p>	

are constructed using the same Cartesian-product scheme with only a minor modification to incorporate  $s$  different singularity coefficients. The singular functions  ${}^e\mathbf{\Lambda}_{i\pm 1}$  and  ${}^e\mathbf{V}_{i+2}$  exhibit the same variation in the parent  $\xi$ -space as that of the zeroth-order vector functions ( $\mathbf{\Lambda}_{i\pm 1}$  or  $\mathbf{\Lambda}_{i+2}$ , respectively) appearing in their expressions, apart the singular factors (2, 3) that are functions of  $\nu$  and  $\xi_i$ . These specific singular factors are only appropriate for the first singular coefficient  $\nu = \nu_1$ . To incorporate a different singularity coefficient  $\nu_n$ , these factors must be modified by adding appropriate *polynomials* of the  $\xi_i$  variable, and imposing the orthogonality relations in Table II, to produce the new singular factors  $f_A(\nu_n) + A_{n-1}$  and  $f_B(\nu_n) + B_{n-1}$ . The order of the polynomials  $A_{n-1}$  and  $B_{n-1}$  depends on  $n$ ; they are of zeroth-order for  $n = 1$  (nothing added), and are of order  $(n-1)$  for  $n \geq 2$ .

The singular hierarchical sets that model higher-order variations along the parent variables are obtained by multiplying the appropriate singular vector factors by a set of orthogonal (shifted-Legendre or modified Jacobi) polynomials. In particular, for  $n \geq 2$ , the  $(n-1)$  coefficients of the polynomials

$$\begin{aligned}
 A_{n-1}(\xi_i) &= \sum_{q=1}^{n-1} a_{q,n-1} \frac{(q+1)(q+2)}{2} [f_A(q+1) - f_A(q)] \\
 &= \sum_{q=1}^{n-1} a_{q,n-1} \frac{(q+1)(q+2)}{2} [(q+1)\xi_i^q - q\xi_i^{q-1}] \quad (5)
 \end{aligned}$$

$$\begin{aligned}
 B_{n-1}(\xi_i) &= \sum_{q=1}^{n-1} b_{q,n-1} \frac{(q+1)(q+2)}{2} [f_B(q+1) - f_B(q)] \\
 &= (\xi_i - 1) \sum_{q=1}^{n-1} b_{q,n-1} \frac{(q+1)(q+2)}{2} \xi_i^{q-1} \quad (6)
 \end{aligned}$$

of Table II associated with  $\nu_n$  are ordered into two column arrays

$$\mathbf{X}_{n-1}^a = \begin{bmatrix} a_{1,n-1} \\ a_{2,n-1} \\ \vdots \\ a_{n-1,n-1} \end{bmatrix}, \quad \mathbf{X}_{n-1}^b = \begin{bmatrix} b_{1,n-1} \\ b_{2,n-1} \\ \vdots \\ b_{n-1,n-1} \end{bmatrix} \quad (7)$$

whose entries depend on the value of the lower order polynomial coefficients, with

$$A_0(\xi_i) = 0 \quad (8)$$

$$B_0(\xi_i) = 0 \quad (9)$$

Eq. (6) forces  $B_{n-1}$  to equal zero at  $\xi_i = 1$  to guarantee that  ${}^e\mathbf{V}_{nk}^{i+2}$  is a bubble function. The coefficients (7) are obtained by imposing the orthogonality of  ${}^e\mathbf{\Lambda}_{nk}^{i\pm 1}$  with respect to the zeroth order polynomial basis functions  $\mathbf{\Lambda}_{i\pm 1}$  and to the other singular functions  ${}^e\mathbf{\Lambda}_{jk}^{i\pm 1}$ , and by imposing the orthogonality of  ${}^e\mathbf{V}_{nk}^{i+2}$  with respect to the other functions  ${}^e\mathbf{V}_{jk}^{i+2}$ , for all

$j = 1, 2, \dots, n-1$ :

$$\int_0^1 [f_A(\nu_n) + A_{n-1}] \begin{bmatrix} P_0(2\xi_i - 1) \\ f_A(\nu_j) + A_{j-1} \end{bmatrix} d\xi_i = \begin{bmatrix} 0 \\ 0 \end{bmatrix} \quad (10)$$

$$\int_0^1 \xi_i^2 [f_B(\nu_n) + B_{n-1}] [f_B(\nu_j) + B_{j-1}] d\xi_i = 0 \quad (11)$$

The normalization coefficients  $N_{n-1}^a$ ,  $N_{n-1}^b$  of the singular basis functions of Table II are obtained by setting

$$N_{n-1}^a \int_0^1 [f_A(\nu_n) + A_{n-1}] P_1(2\xi_i - 1) d\xi_i = 1 \quad (12)$$

$$N_{n-1}^b \int_0^1 \xi_i [f_B(\nu_n) + B_{n-1}] P_0(2\xi_i - 1) d\xi_i = 1 \quad (13)$$

that yield

$$N_{n-1}^a = \left( \frac{\nu_n - 1}{\nu_n + 1} + \sum_{q=1}^{n-1} a_{q,n-1} \right)^{-1} \quad (14)$$

$$N_{n-1}^b = -2 \left( \frac{\nu_n - 1}{\nu_n + 1} + \sum_{q=1}^{n-1} b_{q,n-1} \right)^{-1} \quad (15)$$

The kernels of (11) and (13) are  $\xi_i^2$  and  $\xi_i$ , respectively, because  $\Lambda_{i+2}$  varies linearly with  $\xi_i$  on the parent cell. Obviously, whenever convenient, one can deviate from (13) and use the different normalization

$$N_{n-1}^b \sqrt{\int_0^1 \{\xi_i [f_B(\nu_n) + B_{n-1}]\}^2 d\xi_i} = 1 \quad (16)$$

since the integral in (16) exists. Also, as far as (10) is concerned, recall that on the parent cell  $\Lambda_{i\pm 1}$  is constant with respect to  $\xi_i$  (see Table I); that is, proportional to the shifted Legendre polynomial  $P_0(2\xi_i - 1) = 1$ .

As per the previous expressions, the coefficients (7) are obtained “on the fly” by solving the  $(n-1)$ -order linear systems

$$\underline{\underline{M}}^a \underline{\underline{X}}_{n-1}^a = \underline{\underline{Y}}^a \quad (17)$$

$$\underline{\underline{M}}^b \underline{\underline{X}}_{n-1}^b = \underline{\underline{Y}}^b \quad (18)$$

The entries of  $\underline{\underline{M}}^{a,b}$ ,  $\underline{\underline{Y}}^{a,b}$  (for  $j, q = 1, 2, \dots, n-1$ ) are

$$M^a[j, q] = \frac{(q+1)(q+2)(\nu_j - 1)\nu_j}{(q + \nu_j - 1)(q + \nu_j)} + \underline{\underline{Sm}}^a \cdot \underline{\underline{X}}_{j-1}^a \quad (19)$$

$$Y^a[j] = 2 - \frac{2\nu_j \nu_n}{\nu_j + \nu_n - 1} + \underline{\underline{Sy}}^a \cdot \underline{\underline{X}}_{j-1}^a \quad (20)$$

$$M^b[j, q] = \frac{(q+1)(\nu_j - 1)(2q + \nu_j + 4)}{(q+3)(q + \nu_j + 1)(q + \nu_j + 2)} + \underline{\underline{Sm}}^b \cdot \underline{\underline{X}}_{j-1}^b \quad (21)$$

$$Y^b[j] = \frac{2(\nu_n - 1)(1 - \nu_j)(\nu_n + \nu_j + 4)}{3(\nu_n + 2)(\nu_j + 2)(\nu_n + \nu_j + 1)} + \underline{\underline{Sy}}^b \cdot \underline{\underline{X}}_{j-1}^b \quad (22)$$

where it is understood that the scalar quantities  $\underline{\underline{Sm}}^{a,b} \cdot \underline{\underline{X}}_{j-1}^{a,b}$  and  $\underline{\underline{Sy}}^{a,b} \cdot \underline{\underline{X}}_{j-1}^{a,b}$  vanish for  $j = 1$  (recall that  $A_0 = B_0 = 0$ )

while, for  $j \geq 2$ , the  $q$ -dependent entries of the  $(j-1)$ -order row-arrays  $\underline{\underline{Sm}}^{a,b}$  and  $\underline{\underline{Sy}}^{a,b}$  are

$$\underline{\underline{Sm}}^a[p] = \frac{q(q+1)(q+2)p(p+1)(p+2)}{(p+q-1)(p+q)(p+q+1)} \quad (23)$$

$$\underline{\underline{Sy}}^a[p] = \frac{(1 - \nu_n)\nu_n(p+1)(p+2)}{(p + \nu_n - 1)(p + \nu_n)} \quad (24)$$

$$\underline{\underline{Sm}}^b[p] = \frac{(p+1)(p+2)(q+1)(q+2)}{(p+q+1)(p+q+2)(p+q+3)} \quad (25)$$

$$\underline{\underline{Sy}}^b[p] = \frac{(p+1)(1 - \nu_n)(2p + \nu_n + 4)}{(p+3)(p + \nu_n + 1)(p + \nu_n + 2)} \quad (26)$$

Eqs. (19)-(26) are readily obtained by the fundamental integrals

$$\int_0^1 f_A(x_n) f_A(x_j) d\xi_i = \frac{x_j x_n}{x_j + x_n - 1} - 1 \quad (27)$$

$$\int_0^1 \xi_i^2 f_B(x_n) f_B(x_j) d\xi_i = \frac{(1 - x_n)(1 - x_j)(x_n + x_j + 4)}{3(x_n + 2)(x_j + 2)(x_n + x_j + 1)} \quad (28)$$

As an example, Table IV reports the singular basis functions for  $\{\nu_1, \nu_2, \nu_3\} = \{\frac{1}{2}, \frac{3}{2}, \frac{5}{2}\}$  that correspond to the case of a zero thickness perfectly conducting wedge.

Clearly, when incorporating only one singular exponent  $\nu_1$ , one can use the singular functions of Table I (with  $\nu = \nu_1$ ) with the polynomial subset of order  $p = 0$  (or with higher-order polynomial subsets as desired). To employ two different exponents ( $\nu_1, \nu_2$ ) one has to increase the order of the regular polynomial subset to a minimum of  $p = 1$ . In general, to include  $s$  different singular exponents, the order of the polynomial subset must be at least  $s - 1$ , since one singular factor for  $\nu_s$  contains an  $(s - 1)$ -th order polynomial of the  $\xi_i$  variable.

The hierarchical nature of the Table II bases permits their order to change from one patch to another. That is, the order of the basis within patches that lie along an edge of the structure does not necessarily need to be equal; one can use high-order bases for some of the patches attached to the edges of the structure and lower order basis on the remaining patches. The mixture of orders may be determined by an adaptive refinement strategy [2]-[4].

#### IV. RESULTS FOR SCATTERING FROM INFINITELY THIN PLATES

The edge of an infinitely thin metal structure exhibits a  $0^\circ$  wedge angle and a set of singularity coefficients [1], [5]

$$\{\nu_1, \nu_2, \dots, \nu_j, \dots\} = \left\{ \frac{1}{2}, \frac{3}{2}, \dots, j - \frac{1}{2}, \dots \right\} \quad (29)$$

Table IV presents the three families of singular basis functions associated with the smallest of these coefficients,  $j=1, 2$ , and 3. Numerical results are presented below for two infinitely thin metallic structures: a square plate and a circular disk.

Although there is no exact solution, the square plate facilitates an assessment of the Condition Number (CN) of the MoM system matrix for changing basis order by working on a very simple “structured” mesh, with no curved elements. The

TABLE IV  
SINGULAR BASIS FUNCTION SET FOR  $\{\nu_1, \nu_2, \nu_3\} = \{\frac{1}{2}, \frac{3}{2}, \frac{5}{2}\}$

Basis Functions		Surface Divergences
${}^e\mathbf{\Lambda}_{j0}^{i\pm 1}(\mathbf{r}) = \mathbf{\Lambda}_{i\pm 1}(\mathbf{r}) \mathcal{A}_j(\xi_i)$ ${}^e\mathbf{\Lambda}_{jk}^{i+1}(\mathbf{r}) = \mathbf{\Lambda}_{i+1}(\mathbf{r}) \mathcal{A}_j(\xi_i) \xi_{i+1} f_{k-1}(z)$ ${}^e\mathbf{V}_{j0}^{i+2}(\mathbf{r}) = \mathbf{\Lambda}_{i+2}(\mathbf{r}) \mathcal{B}_j(\xi_i)$ ${}^e\mathbf{V}_{jk}^{i+2}(\mathbf{r}) = \mathbf{\Lambda}_{i+2}(\mathbf{r}) \mathcal{B}_j(\xi_i) E_k(z)$		$\nabla \cdot {}^e\mathbf{\Lambda}_{j0}^{i\pm 1}(\mathbf{r}) = \frac{\mathcal{A}_j(\xi_i)}{\mathcal{J}}$ $\nabla \cdot {}^e\mathbf{\Lambda}_{jk}^{i+1}(\mathbf{r}) = \frac{\mathcal{A}_j(\xi_i)}{\mathcal{J}} g_{k-1}(z)$ $\nabla \cdot {}^e\mathbf{V}_{j0}^{i+2}(\mathbf{r}) = \frac{\mathcal{C}_j(\xi_i)}{\mathcal{J}}$ $\nabla \cdot {}^e\mathbf{V}_{jk}^{i+2}(\mathbf{r}) = \frac{\mathcal{C}_j(\xi_i)}{\mathcal{J}} E_k(z)$
For $k = 1, 2, \dots, p$ with $p \geq 3$ , and $z = \xi_{i+1} - \xi_{i-1}$		For $k = 1, 2, \dots, p$ with $p \geq 3$ , and $z = \xi_{i+1} - \xi_{i-1}$
Use $j = 1$ for the $\nu_1$ set, where $\xi_i^{\nu_1-1} = 1/\sqrt{\xi_i}$ , and $\mathcal{A}_1(\xi_i) = 3 \left(1 - \frac{1}{2\sqrt{\xi_i}}\right)$ $\mathcal{B}_1(\xi_i) = 6 \left(\frac{1}{\sqrt{\xi_i}} - 1\right)$ $\mathcal{C}_1(\xi_i) = 3 \left(\frac{1}{\sqrt{\xi_i}} - 2\right)$	Use $j = 2$ for the $\nu_2$ set, where $\xi_i^{\nu_2-1} = \sqrt{\xi_i}$ , and $\mathcal{A}_2(\xi_i) = 5 \left(6\xi_i - 6\sqrt{\xi_i} + 1\right)$ $\mathcal{B}_2(\xi_i) = 30 \left(13\sqrt{\xi_i} - 8\xi_i - 5\right)$ $\mathcal{C}_2(\xi_i) = 15 \left(39\sqrt{\xi_i} - 32\xi_i - 10\right)$	Use $j = 3$ for the $\nu_3$ set, where $\xi_i^{\nu_3-1} = \xi_i \sqrt{\xi_i}$ , and $\mathcal{A}_3(\xi_i) = \frac{7}{4} \left[10\xi_i \left(82\sqrt{\xi_i} - 51\xi_i - 33\right) + 7\right]$ $\mathcal{B}_3(\xi_i) = \frac{84}{59} \left[\xi_i \left(2584\sqrt{\xi_i} - 1247\xi_i - 1456\right) + 119\right]$ $\mathcal{C}_3(\xi_i) = \frac{84}{59} \left[\xi_i \left(6460\sqrt{\xi_i} - 3741\xi_i - 2912\right) + 119\right]$
<p>The polynomials <math>E</math>, <math>f</math>, and <math>g</math> are given in Table III. For example, for <math>k</math> at most 3, one needs:</p> $E_1(z) = \sqrt{3}z, \quad E_2(z) = \frac{\sqrt{5}}{2} (3z^2 - 1), \quad E_3(z) = \frac{\sqrt{7}}{2} z (5z^2 - 3),$ $f_0(z) = \sqrt{10}, \quad f_1(z) = \sqrt{70}z, \quad f_2(z) = \sqrt{\frac{15}{2}} (7z^2 - 1),$ $g_0(z) = \sqrt{10}z, \quad g_1(z) = \sqrt{\frac{35}{2}} (3z^2 - 1), \quad g_2(z) = \sqrt{30}z (7z^2 - 4).$		
<p>The coefficients of the <math>A_{n-1}(\xi_i)</math> and <math>B_{n-1}(\xi_i)</math> polynomials of Table II and Eqs. (5, 6) are obtained “on the fly”. This Table reports the singular basis function set for <math>\{\nu_1, \nu_2, \nu_3\} = \{1/2, 3/2, 5/2\}</math> to help the reader verify his own implementation of the procedure illustrated in Eqs. (17) - (26).</p>		

versatility of our hierarchical bases is also more easily and intuitively tested by working on such structured meshes.

The second test-case problem we consider is the circular disk because it has no corner and it is one of only a few three-dimensional geometries amenable to exact electromagnetic (EM) analysis [19].

The frequency domain results reported below are obtained by solving the EFIE with hierarchical polynomial basis functions from [11] combined with the singular basis functions reported here in the edge cells. Galerkin testing is used and the equations are solved by standard LU factorization. All necessary integrals are computed by adaptive quadrature. More details on the matrix entry computation are given in a companion paper [12].

#### A. Results for Scattering from an Infinitely Thin Square Plate

Consider an infinitely thin metallic square plate of size  $1\lambda \times 1\lambda$  located in the  $x, y$  Cartesian plane, normally illuminated by a plane wave with unity magnitude  $H$ -field parallel to the  $y$  axis. In most of the examples to follow, the plate is meshed with 25 square cells of equal size  $\lambda/5 \times \lambda/5$ .

Fig. 1 at left shows the magnitude of the  $x$  (co-polarized) component of the current induced on the plate obtained with a  $[2, 1, 0]$  base on a  $5 \times 5$  mesh. This component is singular along the edges located at  $y = \pm\lambda/2$  and vanishes along the other two edges with a square root slope. The co-polarized component is essentially indistinguishable from the *benchmark* solution reported in [20] where the  $x$  and  $y$  components of the current are obtained by the weighed sum of even and odd symmetric functions whose domain is the whole plate. Differences with respect to the benchmark are visible only for the cross-polarized current component shown at the center of Fig. 1, which should be zero along the two symmetry axes of the plate. The vanishing of this component along the symmetry axes is enforced by the functions used to construct the benchmark solution shown at right, whereas, in our simulation, the vanishing occurs in spite of the fact that these symmetry axes divide and run inside the internal elements.

Fig. 2 shows the same current obtained by using the lowest possible polynomial basis subset ( $p = 0$ ) with and without a singular basis term, that is for the orders  $[0, 1, 0]$  and  $[0, 0, 0]$ , respectively. (The functions described by order  $[0, 0, 0]$  are the

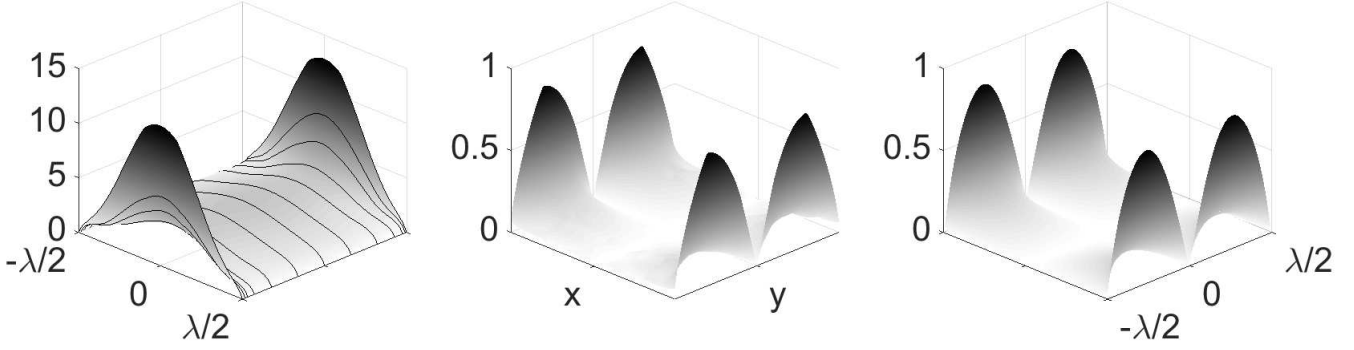


Fig. 1. Magnitude of the current on a  $1\lambda \times 1\lambda$  square plate as induced by a normally incident plane-wave with  $H_y = 1$  A/m. The  $x$  (co-polar) and  $y$  (cross-polar) components of the current at left and center are obtained using a  $[2, 1, 0]$  base with singular basis functions in 16 of the 25 cells of the plate to model only the first singularity exponent  $\nu = 1/2$ . The total number of DoF is 456 (36 singular + 420 polynomial). The results are obtained with Galerkin testing, and the condition number of the resulting MoM matrix is 1,400. The figure at right shows the benchmark solution [20] for the cross-polarized component. The co-polarized benchmark solution is indistinguishable from the results shown at left. Both the  $x$  and  $y$  components are unbounded (when tangent to an edge) at the plate edges even if the rendering of the figure does not show this.

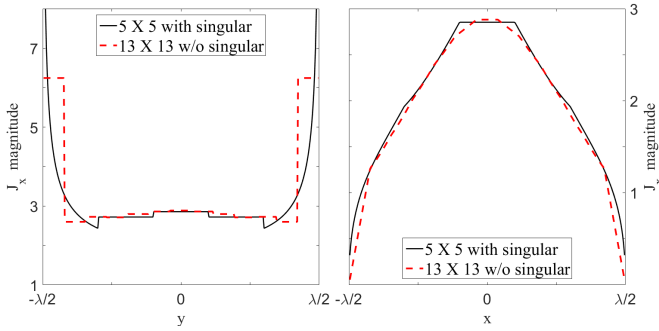


Fig. 2. Normalized magnitude of the current  $x$ -component along the  $x = 0$  (at left) and  $y = 0$  (at right) cut, for the square plate considered in Fig. 1, obtained with zeroth-order polynomial subsets. Meixner basis functions are used only on the cells that are on the border of the plate to get the solid-line results.

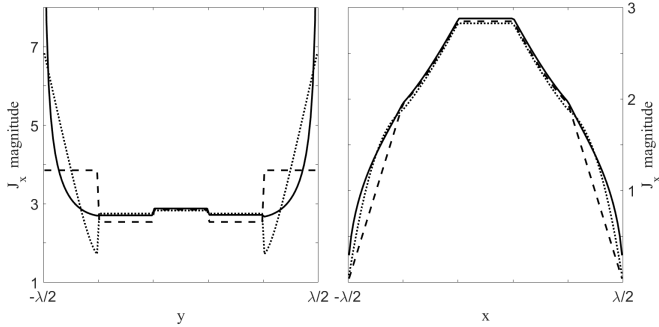


Fig. 3. Normalized magnitude of the current  $x$  component along the  $x = 0$  (at left) and  $y = 0$  (at right) cut, for the square plate considered in Fig. 1, obtained by  $p$ -refinement of the  $p=0$  base.

classical *rooftop* basis and testing functions.) To run the code without the singular terms we used a denser mesh made of 169 equal-size square cells (312 DoF). The results in this figure are not as smooth as might be desired, but they illustrate that similar accuracy is obtained in the currents with only 76 DoF (a matrix with  $1/4$  the order) due to the singular functions.

If we implement  $p$ -refinement we can improve the accuracy with far less than the 312 DoF required by the  $13 \times 13$  cell mesh used to produce Fig. 2. Fig. 3 shows results for the same

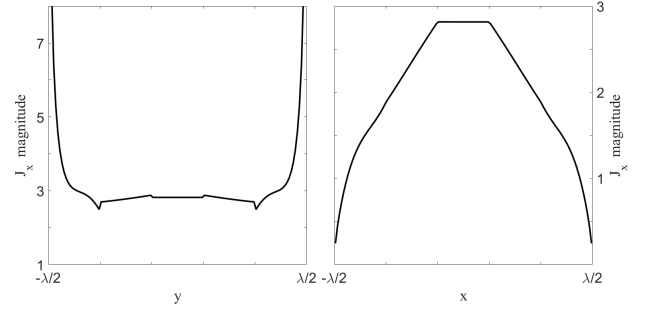


Fig. 4. Normalized magnitude of the current  $x$  component along the  $x = 0$  cut for the same test case of Fig. 1 obtained by using bases of different order in the various cells.

cuts considered in Fig. 2 obtained with bases of different order in the various cells. In particular, we always use the  $p = 0$  base on the nine inner cells and increase the base order only on the 16 outer cells. The “background” results obtained with the purely polynomial  $p=0$  base are shown by dashed-lines (40 DoF). The dotted-line results are obtained after increasing the order in the outer cells to  $p=1$  (120 DoF). (For the edges shared with an internal cell we introduce only the  $p=0$  edge-based functions and discard the  $p=1$  ones so not to spoil the zeroth-order representation used on the inner cells.) Finally, the solid-line results (156 DoF) are obtained by adding the Meixner set to the external cells (an extra 36 singular basis functions), thereby using the  $[1, 1, 0]$  base on these cells only. (Note that for the excitation considered it would be enough to add the singular functions only on the two edges where the singularity is excited, and then add only 18 instead of 36 singular functions. In doing so, the results for the induced current remain essentially the same, but 138 DoF would be used in all, with further savings.) Had we used the first-order ( $p=1$ ) polynomial subset base on all the 25 cells of the mesh plus the Meixner set we would have used 216 DoF. However, this is still less than the 312 DoF used to produce Fig. 2. In spite of the fact that in Fig. 3 the order of the base on the inner cells does not change, the overall solution is improved just by increasing the order of the base used on the outer cells.



Notice also that  $p$ -refinement does not spoil the continuity of the normal component of the current across adjacent cells, as can be clearly seen from Fig. 3 at right.

To illustrate a hierarchical increase of the basis order, Fig. 4 shows the results obtained for a  $5 \times 5$  mesh using a  $p=0$  basis on the central cell, a  $p=1$  basis on the inner ring of cells, and a  $[2, 2, 2]$  basis on the the edge cells. In this case the number of DoFs is 540 instead of the 652 required by a uniform use of the  $p = 2$  order on all 25 cells.

The results that follow employ expansions with identical polynomial order on all cells (with no  $p$ -refinement).

It is of importance to stress that in the absence of singular basis functions (the Meixner subset) the quality of the plate currents is not improved by increasing the order of the polynomial subset. In fact, the current obtained using purely polynomial basis functions shows non-physical oscillations near the singular edges with a pseudo frequency that increases as the order of the polynomial base grows (Fig. 5 at top left). On the contrary (Fig. 5 at top-right), by adding even only one singular basis function these oscillations disappear. In addition, the continuity of the  $x$ -component of the current increasingly improves with the growth of the basis order, despite the fact that divergence-conforming basis functions do not enforce this (expected) tangential continuity across cell borders. Recall that divergence-conforming functions merely force the continuity of the current component normal to the border in common to two adjacent cells, as shown in the figures at bottom of Fig. 5. In fact, the “non-physical” ripples occurring in the absence of singular basis functions can be used in a  $p$ -refinement strategy to identify the cells where it is necessary to refine the representation by adding singular functions.

It is noteworthy that by adding only one (dominant) singular exponent the results obtained with a very coarse mesh appear to outperform commercial codes based on low-order polynomial basis sets, which can require thousands of elements and the solution of very large systems (more than a thousand DoF) even when dealing with scatterers of moderate size (see for example Fig. 5 at right and its caption). An exact solution for this test case does not exist, although our results compare very well with those reported in [10], [20], [21], [22].

Fig. 6 shows the RCS of this plate versus the DoF obtained with three different basis sets. Clearly the convergence is dramatically improved just by adding one singularity (the dominant one) in the numerical model. The addition of the dominant singular term for  $\nu = 1/2$  permits one to obtain good results even with a background representation based on rooftop basis functions.

Table V reports the Condition Number (CN) of the MoM system matrix and the total CPU time obtained using various combinations of polynomial and singular basis subsets for a plate modeled with 25 cells (without  $p$ -refinement). The total (matrix fill-in plus solution) CPU time is normalized to the CPU time spent when using the  $[1,1,1]$  base. The system solution time is negligible with respect to the matrix fill-in time. When in use, the singular basis functions are assigned to the 16 cells along the four plate edges. (In a general structure meshed with a high number of cells, where most cells are not located at an edge, the number of singular DoF is typically lower

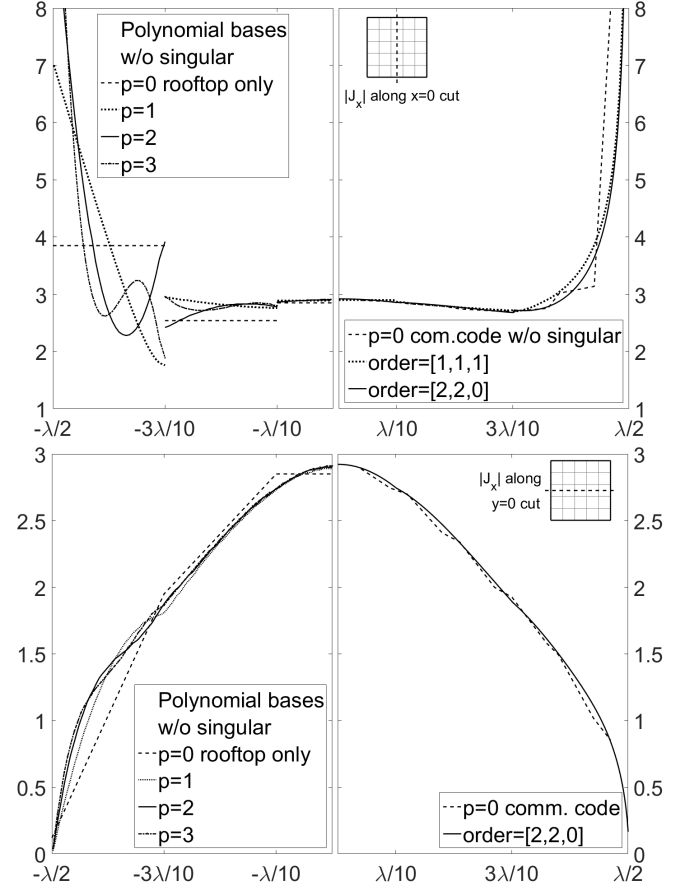


Fig. 5. Normalized magnitude of the current  $x$ -component along the  $x = 0$  (at top) and  $y = 0$  (at bottom) cut, for the same test case of Fig. 1. The results on the left-hand side are obtained with purely polynomial bases. On the right-hand side the results obtained with singular bases are compared against those obtained by a commercial code run by using about 20,000 triangular cells. With singular bases for  $p \geq 1$  the current behavior along the  $y = 0$  cut (at bottom right) does not change appreciably.

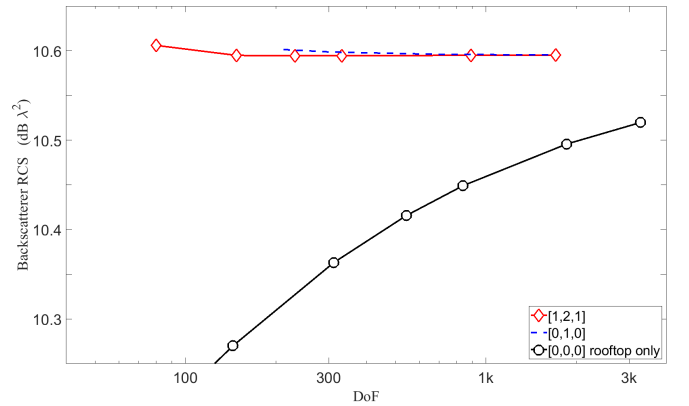


Fig. 6. RCS for the same square plate considered in Fig. 1.

than the number of polynomial DoF. For this 25-cell plate, the singular DoF sometimes exceed the polynomial DoF.) In Table V, for purely polynomial bases, the CN grows slowly with the order. This is due to the fact that the hierarchical polynomial basis functions are linearly independent (in fact, for this rectangular mesh they are actually orthogonal). The

TABLE V  
MATRIX CONDITION NUMBER, CPU TIME, AND NUMBER  
OF DoF FOR THE SQUARE PLATE TEST PROBLEM

Base Order			CN	CN after pre-conditioning	CPU Time (Normalized)
$p$	$s$	$m$			
0	0	0	12	12	0.2
0	1	0	34	25	0.3
0	1	1	83	155	0.6
0	1	2	212	275	0.8
0	2	0	496	69	0.4
0	2	1	$8.3 \times 10^3$	$2.3 \times 10^3$	0.8
0	2	2	$5.0 \times 10^4$	$1.4 \times 10^4$	1.4
<hr/>					
1	0	0	330	363	0.4
1	1	0	690	407	0.7
<b>1</b>	<b>1</b>	<b>1</b>	<b><math>1.8 \times 10^3</math></b>	<b><math>1.3 \times 10^3</math></b>	<b>1.0</b>
1	1	2	$2.9 \times 10^3$	$1.5 \times 10^3$	1.4
1	2	0	$8.0 \times 10^3$	820	0.8
1	2	1	$7.0 \times 10^4$	$9.4 \times 10^3$	1.4
1	2	2	$1.8 \times 10^5$	$2.1 \times 10^4$	2.1
<hr/>					
2	0	0	685	$1.3 \times 10^3$	1.3
2	1	0	$1.3 \times 10^3$	$1.5 \times 10^3$	1.8
2	1	1	$3.4 \times 10^3$	$2.9 \times 10^3$	2.3
2	1	2	$6.0 \times 10^3$	$3.5 \times 10^3$	2.9
2	2	0	$1.5 \times 10^4$	$2.0 \times 10^3$	2.1
2	2	1	$1.9 \times 10^5$	$1.6 \times 10^4$	2.9
2	2	2	$4.6 \times 10^5$	$3.6 \times 10^4$	4.1

Square plate of size  $1\lambda \times 1\lambda$  meshed with  $5 \times 5$  equal square cells. Singular basis and testing functions are used only on the cells that are on the border of the plate. The number of unknowns used by the  $[p, s, m]$  order base is equal to

$$\text{DoF} = 10(p+1)(5p+4) + s(36+40m)$$

The MoM system matrix Condition Numbers (CN) obtained with and without diagonal preconditioning are reported. The last column reports the total (matrix fill-in plus solution) CPU time normalized to the CPU time spent when using the  $[1,1,1]$  base.

CN increases faster when adding the Meixner subset. This suggests that the linear independence of the singular basis functions can be improved, and motivates additional research efforts. A noticeable exception to this trend is observed for bases of order  $[0,1,m]$  because in that case the Meixner basis functions are orthogonal to the zeroth-order polynomial functions. Except for this case, we do not recommend using bases with an order  $s > p+1$ . (For  $s$  fractional exponents, the Meixner functions contain polynomial terms of order  $s-1$ , which exceed the background polynomial order.)

Fig. 7 provides CN and run-time data for the purely polynomial bases of order  $[p,0,0]$ , and singular bases of order  $[p,1,1]$  and  $[p,2,2]$ . The CNs shown in the figure are obtained after calculating the MoM integrals with high precision. We have observed that lower precision integration, while usually yielding an acceptable solution for the induced current, sometimes produces unreliable CNs. In Fig. 7, the CN for the  $[p,p,p]$  bases roughly grows as  $\text{CN}=30 (\text{DoF}/100)^4$ . The CPU time also grows roughly as  $p$  to the fourth power (Fig. 7 at right).

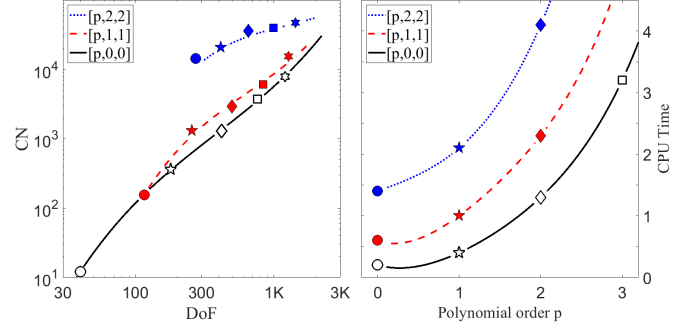


Fig. 7. The square-plate test case. The figure at left shows in logarithmic scale the Condition Number (computed after simple diagonal scaling) versus the number of DoF. The figure at right shows the normalized CPU time versus the polynomial order  $p$  obtained with purely polynomial bases of order  $p$  (solid line), singular bases of order  $[p,1,1]$  (dashed-line), and the  $[p,2,2]$  base (dotted-line). The polynomial subset order is distinguished by different markers: a circle for  $p=0$ , a star for  $p=1$ , a diamond for  $p=2$ , a square for  $p=3$ , and a six-pointed star for  $p=4$ . The CPU times are normalized with respect to the time spent in solving the problem with the  $[1,1,1]$  order base (red star marker).

### B. Results for Scattering from a Circular Disk

A circular, perfectly conducting disk is one of only a few three-dimensional geometries amenable to exact electromagnetic (EM) analysis [19]. As such, the disk offers the potential to serve as a benchmark for validating EM modeling software, and specifically for studying the performance of special numerical techniques for accurately modeling edge singularities. A disk of radius  $a$  can be discretized by (curved) quadrilateral cells.

Fig. 8 shows the normalized magnitude of the co-polarized current component induced on disk with  $ka = 2\pi$  (at left) and  $ka = 10$  (at right) by a normally incident plane wave with unity magnitude  $H$ -field, for two cuts through the disk center along the  $y$  and  $x$ -axis. The results, compared with the exact solution, are obtained with a zeroth order pure polynomial basis subset (roof top basis functions) augmented with singular basis functions that model only the first (dominant) singular coefficient  $\nu = 1/2$  (that is, by using the singular functions of Table I for  $p = 0, s = 1, m = 0$ ). This figure clearly shows that acceptable results are obtainable with a low-order basis by including just the functions that model the first dominant singularity.

Fig. 9 shows the 2-norm error in the bistatic RCS of the disk with  $ka = 2\pi$  for a normally-incident wave, for a series of meshes and three sets of basis functions, two of which employ singular functions in the edge cells. The 2-norm error is measured every 30 degrees in  $\theta$  and  $\phi$ . An order of magnitude improvement in accuracy is observed when the singular basis functions are employed.

## V. CONCLUSION

Hierarchical vector basis functions are proposed for modeling edge singularities in quadrilateral cells. The functions are described in detail, and results for perfectly conducting square plates and circular disks are used to illustrate the improved accuracy and efficiency of the bases. The increase in matrix

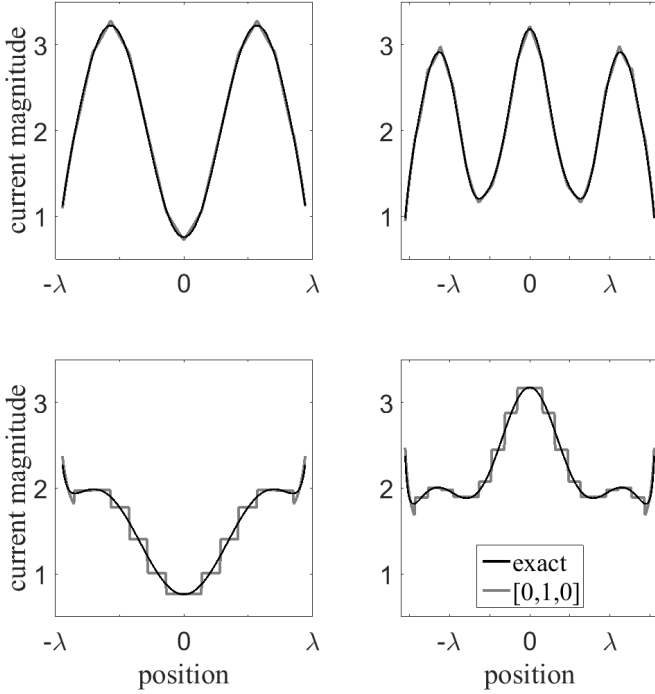


Fig. 8. The figures at left show the co-polarized current induced on a disk with  $ka = 2\pi$  by a normally incident plane wave with unity magnitude  $H$ -field. The numerical result incorporating singular basis functions in the edge cells for a 192-cell mesh is shown for cuts through the disk center along the co-polarized (at top) and cross-polarized (at bottom) axes. The figures at right show the analogous current induced on a disk with  $ka = 10$  by a normally incident plane wave, for a 336-cell mesh.

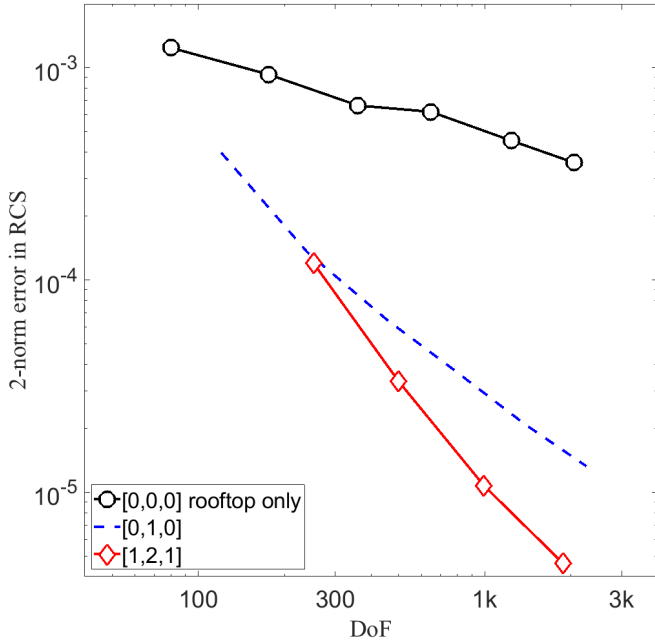


Fig. 9. 2-norm error in the bistatic RCS of the disk with  $ka = 2\pi$  for a normally-incident wave, for a series of meshes employing bases with and without singular functions in the edge cells. The 2-norm error is measured every 30 degrees in  $\theta$  and  $\phi$ .

## REFERENCES

- [1] J. Van Bladel, *Singular Electromagnetic Fields and Sources*. Oxford, U.K.: Clarendon, 1991.
- [2] M. Salazar-Palma, T. K. Sarkar, L.-E. Garcia-Castillo, T. Roy, and A. Djordjevic, *Iterative and Self-Adaptive Finite-Elements in Electromagnetic Modeling*. Boston, Artech House, 1998.
- [3] L. Demkowicz, *Computing with hp-Adaptive Finite Elements*, vol. 1. Boca Raton, Chapman & Hall/CRC, 2007.
- [4] L. Demkowicz, *Computing with hp-Adaptive Finite Elements*, vol. 2. Boca Raton, Chapman & Hall/CRC, 2008.
- [5] A. F. Peterson, and R. D. Graglia, "Basis Functions for Vertex, Edge, and Corner Singularities: A Review," invited paper, *IEEE Journal on Multiscale and Multiphysics Computational Techniques*, vol. 1, pp. 161 - 175, 2016.
- [6] W. J. Brown and D. R. Wilton, "Singular basis functions and curvilinear triangles in the solution of the electric field integral equation," *IEEE Trans. Antennas Propagat.*, vol. 47, pp. 347-353, Feb. 1999.
- [7] R.D. Graglia, G. Lombardi, Singular Higher-Order Complete Vector Bases for Finite Methods, *IEEE Trans. Antennas Propagat.*, vol. 52, pp. 1672-1685, 2004.
- [8] A. K. Ozturk, R. Paknys, and C. W. Trueman, "First-order singular basis functions for corner diffraction analysis using the method of moments," *IEEE Trans. Antennas Propagat.*, vol. 57, pp. 3160-3168, Oct. 2009.
- [9] T. Andersson, "Moment method calculations of scattering by a square plate using singular basis functions and multipole expansions," *J. Electromagnetic Waves Appl.*, vol. 7, pp. 93-121, 1993.
- [10] R. D. Graglia, and G. Lombardi, "Singular higher order divergence-conforming bases of additive kind and moments method applications to 3D sharp-wedge structures," *IEEE Trans. Antennas Propagat.*, vol. 56, no. 12, pp. 3768 - 3788, Dec. 2008.
- [11] R. D. Graglia, and A. F. Peterson, *Higher-order Techniques in Computational Electromagnetics*, 392 pages, SciTech Publishing/IET, Edison, NJ, 2016.
- [12] R. D. Graglia, A. F. Peterson, and P. Petrini, "Computation of EFIE Matrix Entries with Singular Basis Functions," *IEEE Trans. Antennas Propagat.*, submitted, Apr. 2018.
- [13] R. D. Graglia, D. R. Wilton and A. F. Peterson, "Higher order interpolatory vector bases for computational electromagnetics," special issue on "Advanced Numerical Techniques in Electromagnetics," *IEEE Trans. Antennas Propagat.*, vol. 45, no. 3, pp. 329-342, Mar. 1997.
- [14] R. D. Graglia, A. F. Peterson, and P. Petrini, "Application of high-order singular hierarchical divergence-conforming bases functions for quadrilateral elements to solve the flat plate problem," 2017 USNC-URSI Radio Science Meeting, San Diego, California, USA, Jul. 2017.
- [15] R. D. Graglia, A. F. Peterson, and P. Petrini, "Hierarchical Singular Vector Bases for Quadrilateral Cell MoM Applications," Proceedings of the 17th International Conference on Electromagnetics in Advanced Applications (ICEAA17), 11-15 Sept., Verona, Italy, 2017.
- [16] G. Lombardi, R.D. Graglia, Modeling junctions in sharp edge conducting structures with higher order method of moments. *IEEE Trans. Antennas Propagat.*, vol. 62, pp. 5723-5731, 2014.
- [17] M. Abramowitz, and I. Stegun, *Handbook of Mathematical Functions*, New York, Dover, 1968.
- [18] R.S. Satterwhite, R.G. Kouyoumjian, *Electromagnetic Diffraction by a Perfectly-Conducting Plane Angular Section*, Sci. Rep. n. 2, contract n. AFL9(628)-5929, Project n. 5635, The Ohio State University, Electro-Science Laboratory, March 23, 1970.
- [19] A. F. Peterson and M. M. Bibby, "Electromagnetic Scattering from a Circular Disk: Use of Flammer's Solution to Assess Numerical Techniques Incorporating Singular Expansions," *IEEE Trans. Antennas Propagat.*, in review, 2018.
- [20] B. M. Kolundzija, "Accurate solution of square scatterer as benchmark for validation of electromagnetic modeling of plate structures," *IEEE Trans. Antennas Propagat.*, vol. 46, n. 7, pp. 1009-1014, Jul. 1998.
- [21] R. Sega, V. Martin, and R. Burton, "Microwave induced surface current measurement via infrared detection," *IEEE Antennas and Propagation Society International Symposium*, Vol. 20, p. 231, 1982.
- [22] R. Sega, *Infrared detection of microwave induced surface current on flat plates*, Unites States Air Force Academy report RADC-TR-82-308, pp. 1-367, 1982.

condition number resulting from the use of singular functions is also reported.



**Roberto D. Graglia** (S'83-M'83-SM'90-F'98) received the Laurea degree (*summa cum laude*) in electronic engineering from the Polytechnic of Turin in 1979, and the Ph.D. degree in electrical engineering and computer science from the University of Illinois at Chicago in 1983. From 1980 to 1981, he was a Research Engineer at CSELT, Italy. From 1981 to 1983, he was a Teaching and Research Assistant at the University of Illinois at Chicago. From 1985 to 1992, he was a Researcher with the Italian National Research Council (CNR). In 1991 and 1993, he was Associate Visiting Professor at the University of Illinois at Chicago. In 1992, he joined the Department of Electronics and Telecommunications, Polytechnic of Turin, as an Associate Professor. He has been a Professor of Electrical Engineering at that Department since 1999. His areas of interest comprise numerical methods for high- and low-frequency electromagnetics, theoretical and computational aspects of scattering and interactions with complex media, waveguides, antennas, electromagnetic compatibility, and low-frequency phenomena. He has organized and offered several short courses in these areas. He is a co-author of the 2016 text *Higher-order Techniques in Computational Electromagnetics*.

Since 1997, he has been a Member of the editorial board of *Electromagnetics*. He served as Associate Editor for the *IEEE Transactions on Antennas and Propagation*, the *IEEE Transactions on Electromagnetic Compatibility*, and the *IEEE Antennas and Wireless Propagation Letters*. He was the Guest Editor of a special issue on Advanced Numerical Techniques in Electromagnetics for the *IEEE Transactions on Antennas and Propagation* in March 1997. Since 1999, he has been the General Chairperson of the International Conference on Electromagnetics in Advanced Applications (ICEAA), and, since 2011, he has been the General Chairperson of the IEEE-APS Topical Conference on Antennas and Propagation in Wireless Communications (IEEE-APWC). Dr. Graglia was the President of the IEEE AP-S during 2015. He is a Fellow of the IEEE, and has been an IEEE AP-S Distinguished Lecturer (2009-2012).



**Paolo Petrini** was born in Torino, Italy, on October 4, 1955. He received the Laurea degree (*summa cum laude*) in electronic engineering from the Polytechnic of Turin in 1979 with a graduation thesis on Integrated Optics and Ph.D. degree in electrical and electronic engineering (*cum laude*) from the Polytechnic of Turin in 2018. In years 1980-81 he was Research Engineer at CSELT, Italy, studying and measuring microwave subsystems for high speed PSK radio links, while in years 1981-82 was Research Engineer at CERN (European Center for Nuclear Research, Geneva, Switzerland) involved in studying and measuring high Q cavities for beam acceleration. From 1983 to 2012 he worked as a registered engineer working in the fields of RF-Microwave and Aerospace engineering, with customers amongst the most important Companies in Europe. Since 2012 he is research assistant at the Department of Electronics and Telecommunications of the Polytechnic of Turin.



**Andrew F. Peterson** (S'82-M'83-SM'92-F'00) received the B.S., M.S., and Ph.D. degrees in electrical engineering from the University of Illinois at Urbana-Champaign in 1982, 1983, and 1986, respectively. Since 1989, he has been a member of the faculty of the School of Electrical and Computer Engineering at the Georgia Institute of Technology, Atlanta, where he is a full Professor. He teaches electromagnetic field theory and computational electromagnetics, and conducts research in the development of computational techniques for electromag-

netic scattering, microwave devices, and electronic packaging applications. He is a co-author of the 1998 text *Computational Methods for Electromagnetics*, the 2016 text *Higher-order Techniques in Computational Electromagnetics*, and several lectures in the Morgan/Claypool Synthesis Library.

Dr. Peterson previously served as General Chair of the 1998 IEEE AP-S International Symposium and URSI/USNC Radio Science Meeting, as a member of IEEE AP-S AdCom, as Chair of the IEEE Atlanta Section, and as a Director of the Applied Computational Electromagnetics Society (ACES). He is currently a Track Editor for the *IEEE Transactions on Antennas and Propagation*, and previously served as Associate Editor for the *IEEE Transactions on Antennas and Propagation* and the *IEEE Antennas and Wireless Propagation Letters*. He was the President of the IEEE AP-S during 2006, and the President of ACES from 2011 to 2013. He is a Fellow of the IEEE, a Fellow of ACES, and a recipient of the IEEE Third Millennium Medal. He is also a member of the International Union of Radio Scientists (URSI) Commission B, the American Society for Engineering Education, and the American Association of University Professors.